Psychiatry Research: Neuroimaging 283 (2019) 67–76

Contents lists available at ScienceDirect

Psychiatry Research: Neuroimaging

journal homepage: www.elsevier.com/locate/psychresns

FMRI correlates of olfactory processing in typically-developing school-aged children

Natalia M. Kleinhans[a,b,c,*], Melissa Reilly[a], Matthew Blake[a], Gabriella Greco[a], Julia Sweigert[a], Greg E. Davis[d], Francisco Velasquez[a], Fredrick Reitz[c], Dennis Shusterman[e], Stephen R. Dager[a,c,f]

[a] Department of Radiology, University of Washington, Seattle, WA, United States
[b] Integrated Brain Imaging Center, University of Washington, Seattle, WA, United States
[c] Center on Human Development and Disability, University of Washington, Seattle, WA, United States
[d] Department of Otolaryngology, University of Washington, Seattle, WA, United States
[e] Department of Medicine, University of California, San Francisco, San Francisco, CA, United States
[f] Department of Biomedical Engineering, University of Washington, Seattle, WA, United States

ARTICLE INFO

Key words:
fMRI
Sensory processing
Odor detection
Olfactory brain circuitry
PEA
Phenyl ethanol
Phenyl ethyl alcohol

ABSTRACT

Human olfactory processing is understudied relative to other sensory modalities, despite its links to neurodevelopmental and neurodegenerative disorders. To address this limitation, we developed a fast, robust fMRI odor paradigm that is appropriate for all ages and levels of cognitive functioning. To test this approach, thirty-four typically developing children aged 7–12 underwent fMRI during brief, repeated exposure to phenylethyl alcohol, a flower-scented odor. Prior to fMRI scanning, olfactory testing (odor detection and identification) was conducted. During fMRI stimulus presentation, odorant release was synchronized to each participant's inspiratory phase to ensure participants were inhaling during the odorant exposure. Between group differences and correlations between activation and odor detection threshold scores were tested using the FMRIB Software Library. Results demonstrated that our 2-min paradigm significantly activated primary and secondary olfactory regions. In addition, a significant relationship between odor detection threshold and higher activation in the right amygdala and lower activation in the left frontal, insular, occipital, and cerebellar regions was observed, suggesting that this approach is sensitive to individual differences in olfactory processing. These findings demonstrate the feasibility of studying olfactory function in children using brain imaging techniques.

1. Introduction

Relationships observed between olfactory dysfunction and both neurological and psychiatric disorders support the importance of understanding the neural correlates of olfactory function. Olfactory dysfunction has been linked to brain-based disorders that emerge across the life span, including depression (Croy et al., 2014; Pause et al., 2001), autism spectrum disorder (Hilton et al., 2010), schizophrenia (Moberg et al., 1999; Woodberry et al., 2010), Parkinson's Disease (Doty, 2007; Iannilli et al., 2017), and dementia (Atanasova et al., 2008; Murphy et al., 1990). Despite these links to neurological and psychiatric disorders both in children and adults, imaging research to elucidate the developmental patterns of olfactory processing has been limited relative to other sensory systems (Wang et al., 2014).

Functional magnetic resonance imaging (fMRI) is increasingly being leveraged in developmental research to assess how neural functioning during childhood and adolescence relates to psychiatric disorders (e.g., Daivs, 2006; Dapretto et al., 2006; Forbes et al., 2006; Levitin et al., 2003), developmental stage (Pruett et al., 2015) and to improve diagnosis (e.g., Emerson et al., 2017; Luking et al., 2011; Philipsen, 2006). FMRI research focused on brain regions involved in olfaction can potentially help to bridge gaps in our knowledge of the role abnormal olfactory processing plays in the etiology of neurodevelopmental disorders. Few studies, however, have used fMRI to study olfaction at specific developmental stages during childhood. This, in part, may reflect the combined methodological challenges of obtaining strong, and robust Blood Oxygen Level Dependent (BOLD) signal response to olfactory stimulation and the difficulties of conducting imaging studies on children. Research on olfactory perception must manage the technical challenges linked to rapid habituation or desensitization to odorants (Poellinger et al., 2001; Sobel et al., 2000), which can rapidly decrease the strength of the BOLD signal response. Further, aside from

* Corresponding author at: Department of Radiology, University of Washington, Box 357115, Seattle, WA 98195, United States.
E-mail address: nkleinha@uw.edu (N.M. Kleinhans).

https://doi.org/10.1016/j.pscychresns.2018.11.011
Received 8 May 2018; Received in revised form 29 November 2018; Accepted 30 November 2018
Available online 02 December 2018
0925-4927/

physiological differences, children exhibit greater head motion (Power et al., 2014), and may experience greater anxiety during the protocol than adults; thus, acclimation to the scanning environment and head motion training is critical to success of the study (Davidson et al., 2003). Moreover, researchers must develop tasks that are suited for the cognitive abilities and attention span of a younger sample (Davidson et al., 2003).

The current study describes an experimental design that demonstrates the feasibility of obtaining robust fMRI responses to an olfactory stimulus from a sample of typically developing school-aged children from 7 to 12 years of age. Activation targets included the primary olfactory cortex (POC), comprising of a set of integrated brain regions (piriform cortex, periamygdalaloid region, anterior and posterior nuclei, nucleus of the lateral olfactory tract, the medial nucleus and the entorhinal cortex) with direct input from the olfactory bulb that detect, identify, and evaluate odors (Gottfried and Zald, 2005; Iannilli et al., 2013; Mori and Sakano, 2011) and secondary olfactory cortex (SOC), which is comprised of brain regions that do not receive direct input from the olfactory bulb (lateral orbital frontal cortex [OFC], medial OFC, insular cortex, hippocampus, lateral nucleus of the amygdala, and the thalamus) but are involved in higher-order odor-related processing, such as behavior regulation, reward processing, memory, and emotional response (de Olmos et al., 1978; Gottfried and Zald, 2005; Martinez-Marcos, 2009). The experimental procedure employed an olfactometer that can deliver discrete and quantifiable olfactory stimuli, a short fMRI protocol that is both suitable for imaging children and limits the potential of rapid habituation to olfactory stimuli, and individualized timing of odorant release to maximize the effect of the stimulus. We additionally investigated whether there was a relationship between patterns of brain activation to the odorant stimuli and participant's olfactory detection threshold measured using the Sniffin' Sticks task (Hummel et al., 2007, 1997), which quantitatively assessed the concentration at which a person can identify the presence of an odorant. Odor detection is dependent on the intact functioning of olfactory receptors, the olfactory bulb, and POC. Thus, we predicted robust activation within the POC and SOC in response to the odorant stimuli, and that a lower odor detection threshold would be associated with increased activation within the POC.

2. Methods

2.1. Participants

Families were recruited from a research registry at the University of Washington, by advertising on our laboratory website, and by posting information on a list serve that target parents in neighborhoods throughout Seattle. Participants were excluded from this study if a parent reported that the child had any current or past odor processing problems, psychiatric disorders, history of a developmental learning disability, and for contraindications to MR imaging (including braces). On the day of the visit, participants were further screened to ensure they did not exhibit symptoms of upper airway breathing disorders or acute cold symptoms. Participants who did exhibit these symptoms were rescheduled for a later date. Thirty-four typically developing (TD) children participated in the study. Six participants were excluded because of excessive head motion during imaging (see below for criteria), two participants decided to terminate the scan before all the sequences were collected, and one left-handed participant was excluded from analysis due to potential effects of handedness on processing pleasant odors (Gottschlich and Hummel, 2015). The final sample consisted of 25 TD participants (6 females, 19 males) ranging in age from 7 to 12 years of age (see Table 1). The study was approved by the Human Subjects Institutional Review Board at the University of Washington and written informed consent was obtained from a parent or guardian. Written assent was obtained from all participants. All clinical investigation was conducted according to the principles expressed in the Declaration of Helsinki.

Table 1
Characteristics of included participants (N = 25).

	M (SD)	Range
Age	10.1 (1.4)	7.8–12.9
Verbal IQ (WASI[a])	117.5 (14.0)	89–139
Performance IQ (WASI[a])	114.6 (14.8)	80–145
Full Scale IQ (WASI[a])	118 (13.0)	83–147
Threshold Test raw score (Sniffin Sticks)	9.1 (4.2)	1.5–14.8
Threshold Test t value (Sniffin Sticks)	61 (20.5)	27–87
Smell Identification Test raw score (UPSIT[b])	30 (3.4)	23–37
Smell Identification Test t value (UPSIT[b])	46 (7.3)	33–64

Note. The sex distribution for our sample was 6 females and 19 males.
[a] Wechsler Abbreviated Scale of Intelligence.
[b] University of Pennsylvania Smell Identification Test.

2.2. Behavioral and odor sensory assessment

Participants first underwent an assessment of cognitive and olfactory performance. Cognitive ability was estimated using the Wechsler Abbreviated Scale of Intelligence (WASI; Wechsler, 1999). Cognitive ability, though widely distributed, was within the normal range in our final sample (Table 1). Olfactory detection threshold was determined using the Threshold Test from the Sniffin' Sticks test battery (Hummel et al., 1997) that utilizes scented pens with 16 dilutions to systematically determine an individual's threshold for detecting smell. We used the phenyl ethyl alcohol odorant version for this study. At each level of dilution, participants are asked to smell the scented pen and two unscented "blanks" to identify which of the three contains the odorant. Subjects proceed through the dilutions in a forced staircase procedure to determine the lowest concentration at which the odorant can be distinguished from the blanks. In addition, participants were administered the University of Pennsylvania Smell Identification Test (UPSIT) (Doty et al., 1984), a 40-item "scratch and sniff" test designed to measure each participant's smell identification ability. Performance scores for each test are reported in Table 1. None of our participants reported impaired olfactory processing during our screening and interview process. Although the majority of our participants performed in the normal range on quantitative measures of olfactory detection threshold (Hummel et al., 1997) and identification ability (Doty et al., 1984), 5/20 performed in the mildly microsmic (UPSIT) and hyposmic (Sniffin' Sticks) range.

2.3. fMRI and task procedure

On a separate visit, functional MRI data were collected using an olfactory stimulus protocol, following acquisition of structural images (see below). During the fMRI task, participants were asked to stare at a black, empty screen inside the scanner and instructed to breathe normally while a stream of air and/or odorant was delivered on a timed schedule via the olfactometer (described in further detail below). To help the children stay still, inflatable stabilizing caps and foam padding were used during fMRI collection.

The fMRI olfactory stimulus protocol employed a block design with four 9-sec olfactory trials separated by an inter-trial interval (ITI) of 18 s plus an adjustment time equal to one half the length of each participant's respiratory cycle (according to the methods reported in Wang et al., 2014), resulting in a minimum possible task duration of 1 min and 48 s (Table 2). This short protocol was employed to limit habituation to the odor.

To determine the length of the ITI adjustment, subjects' breathing rates were monitored during collection of the structural scan using a respiratory strain-gauge belt. The belt transmitted a signal to the Invivo Precess system, which was connected to a National Instruments (NI;

Table 2
Duration lengths by stimulus-type for the fMRI olfactory scan.

	Mean (N = 25)	Minimum	Maximum	SD
ITI (s)	20.5	19.1	22.1	0.7
Odor block (s)	9.0	9.0	9.0	0
Total run (s)	119.5	114.2	135.0	4.1

Austin, Texas) BNC-2090A breakout box and digitized by a NI PCI-6259 A/D device, and then ported into National Instruments (NI) LabVIEW™ software using NI BNC-2090A connectors. Custom NI LabVIEW software was employed to process, filter, and monitor the output of the Invivo Respiration system and calculate a unique "peak-to-scent delay" estimation for each participant (Fig. 1; software available upon request). This delay is equal to one half of the average time required by a participant to cycle through one inhalation and exhalation (peak-to-scent delay = $\frac{\text{full peak} - \text{to} - \text{peak cycle}}{2}$). These data were then used to customize timing of the odorant stimulus release during fMRI acquisition. Specifically, the custom NI LabVIEW software detected the next respiration peak (maximum of inhalation) after the 18-sec ITI, then used the previously determined peak-to-scent delay to estimate half of the subject's respiratory cycle (exhalation phase) before automatically triggering the olfactometer release of the scent, such that odorant exposure was timed to the onset of the participant's next inhalation.

Pure phenylethyl alcohol (concentration ≥99% v/v; Sigma-Aldrich) mixed with plain air was used as the olfactory stimulus (methods are described in Section 2.4 Olfactory details). This rose-like odorant is generally considered to be a selective olfactory stimulant (Doty et al., 1978; Frasnelli et al., 2011) processed by the POC and olfaction-related areas of the OFC, without activating the somatosensory trigeminal system (Yousem et al., 1997). 0.05 mL of the odorant was dropped onto a 1-inch diameter filter paper and placed in the odorant chamber of the olfactometer. All participants had previous exposure to this odorant during the odor detection threshold task.

2.4. Olfactometer details

The intent of the olfactometer design was to allow rapid switching between olfactory stimuli without interrupting the flow of air. To do so would impart an intermittent mechanical stimulus to the nasal mucosa, which could act as a confounding sensory input underlying any fMRI activation. The design also ensures that no auditory stimuli coincided with olfactory stimulus switching by locating the solenoid valves outside of the scanner room; the high ambient noise in the fMRI suite also masked any auditory stimuli.

The olfactometer design was based on Lorig et al. (1999), with modification of the odorant cylinders/manifold and nosepiece. Air from a compressor (DeVilbiss Pulmo-Aide) was passed through a Drierite Gas Drying unit and a 0.3μ nylon filter before splitting into two pathways: Constant Flow and Odor/No Odor (see Fig. 2). One Flowmeter (Cole-Parmer, # RK-32003-10) on each pathway controlled air flow rate. Air moved continuously through the Constant Flow path at a rate of 0.5 L/min via a normally-open solenoid valve (Cole Parmer #EW-01540-09, Vernon Hills, IL) to the nosepiece for the length of the entire fMRI protocol. The Odor/No Odor pathway used a 6-in-1-out solenoid manifold (Cole-Parmer #RK-01356-16), driven by a USB-controlled relay array (Measurement Computing SwitchAndSense-8/8, Norton, MA) directed by our custom LabVIEW™ software, to send air at 1.25 L/min through either the Control Flow (no odor) path during the ITI or the odorant-containing chamber during 9-sec stimulus block. The Constant Flow, Control Flow and Odorant pathways merged at the nosepiece delivery tube, which was mounted on the head coil adjacent to the participant's nose. Care was taken to verify that the flow rate did not differ upon switching between the control and odorant paths to within the precision of the flowmeters when tested with minimal (<1 m) tubing lengths. Any undetected difference would thus also have

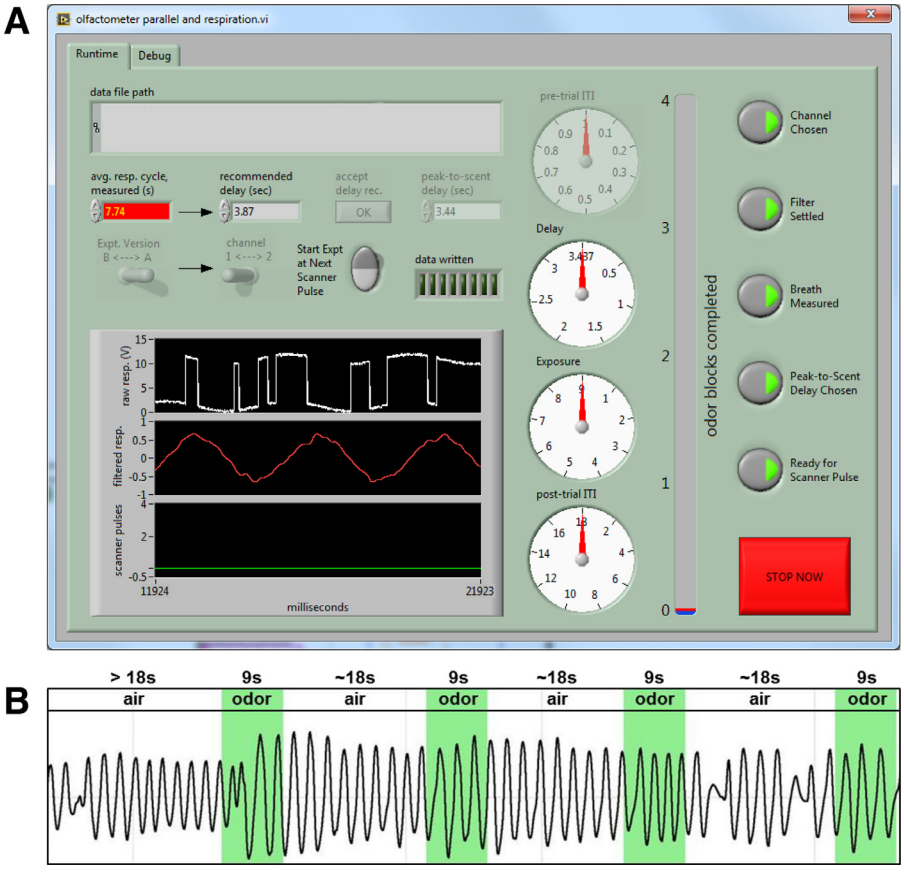

Fig. 1. Respiratory software. (A) Example screenshot of the olfactometer software display showing average respiratory cycle, peak-to-scent delay and other customizable controls. Upper left of screen shows where each subject's unique peak-to-scent delay is calculated. (B) Respiratory trace for a representative subject's entire fMRI run. Timing of odor exposure is superimposed in green. (For interpretation of the references to color in this figure legend, the reader is referred to the web version of this article.)

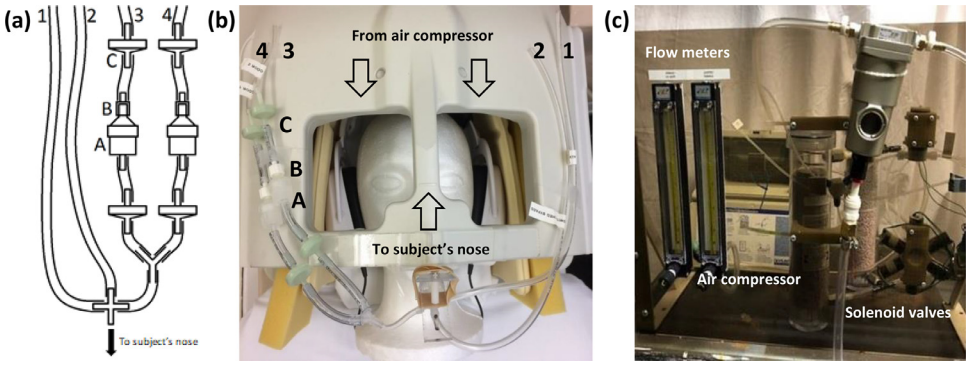

Fig. 2. The revised olfactometer manifold. (2.a) and (2.b) Tubes 1 and 2 correspond respectively to the "Constant Flow" and "Control Flow" tubes described in Lorig et al. (1999). Two odorant channels (tubes 3 and 4) are shown, in which the odorant was places in a filter holder (A) coupled to the tubing by a Luer adapter (B) and flanked by check valves (C). All tubing came together at a T coupler with the output tube attached to the headcoil adjacent to the subject's nose. (2.c) Labeled diagram of the air compressor connected to flow meters and solenoids that output air flow to tubes 1 and 2 or, when dispensing odorant, tubes 1, 3, and 4.

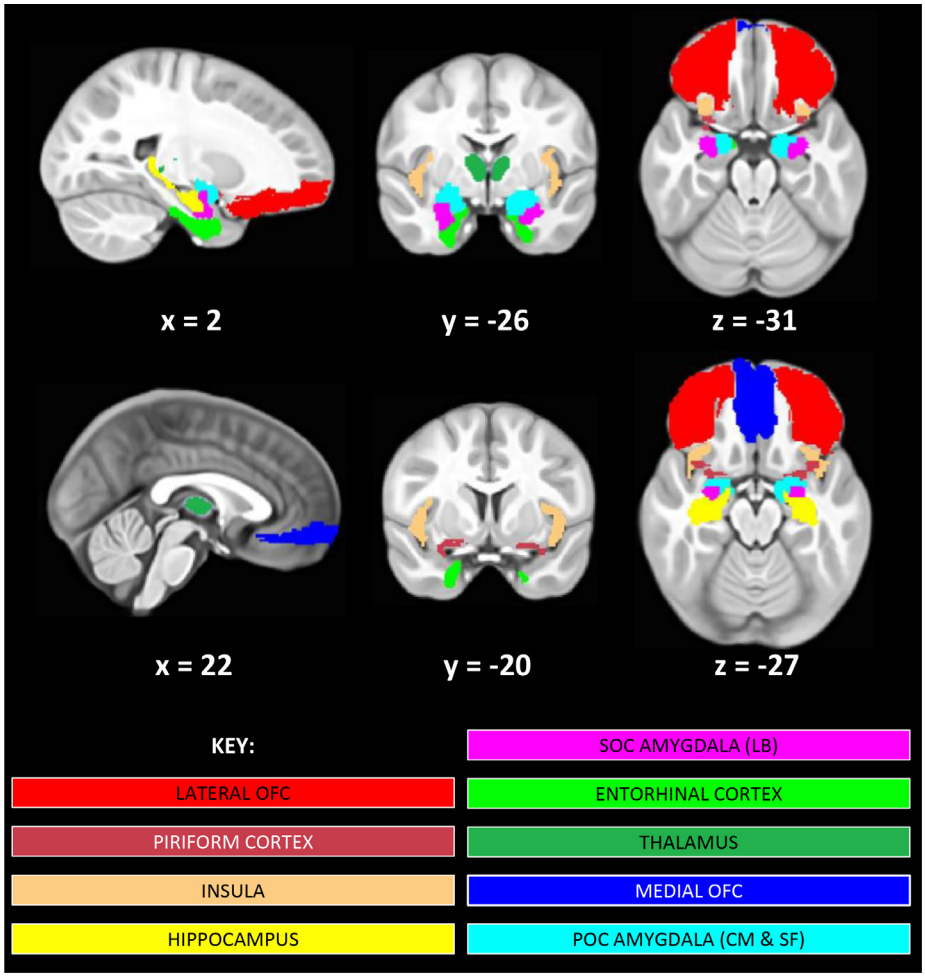

Fig. 3. Masks of primary olfactory cortex (POC) and secondary olfactory cortex (SOC) regions analyzed. Brain images display medial orbital frontal cortex (OFC; dark blue), lateral OFC (red), insular cortex (peach), piriform cortex (burgundy), POC amygdala (centromedial (CM) and superficial (SF) subregions; light blue), SOC amygdala (laterobasal (LB) subregion; magenta), hippocampus (yellow), entorhinal cortex (lime green), and thalamus (dark green) masks shown on our study-specific 34 pediatric template. Images are shown in radiological convention (R = L). Left and right hemisphere masks for each of these regions of interest were analyzed separately except for the medial OFC. (For interpretation of the references to color in this figure legend, the reader is referred to the web version of this article.)

been greatly further attenuated in use with a subject, as the resistance to flow of the system is by far dominated by the ~15 m lengths of narrow-bore tubing used to convey the air into the MRI bore, with path differences within the manifold itself playing a negligible role. Preliminary testing showed that this mounted delivery tube, as opposed to the nasal cannula or oxygen mask designs seen in other studies, was easier for children to tolerate.

2.5. Imaging data acquisition

Structural and functional MRI data were acquired on a 3T Philips Achieva scanner (version 1.5, Philips Medical Systems, Best, The Netherlands) with Quasar dual gradients using a 32-channel SENSE head coil. A T1-weighted 3DMPRAGE (magnetization prepared-rapid gradient echo); TR 7.6 ms; TE 3.6 ms; flip angle = 7, FOV = 176 mm, matrix 176 × 256, 176 slices, acquisition voxel size (mm^3) = 1.00/1.00/1.00; reconstruction voxel size = (mm^3) = 1.00/1.00/1.00; TFE shots = 128; TFE durations = 1963.3 ms; Inversion delay (TI) 910.5 ms; slice orientation transverse, fold-over direction AP; REST slab 64.2 mm slice thickness) was collected for fMRI co-registration and anatomical localization.

The fMRI acquisition parameters were as follows: TR 3000 ms; TE 21 ms; flip angle = 90°, FOV = 224 mm, matrix 96 × 96, 58 slices, acquisition voxel size (mm^3) = 2.33/2.33; slice thickness: 2.33 (mm), 0 gap. Because the odorant stimulus blocks were triggered according to individual respiration patterns, the number of volumes collected varied by participant, and ranged from 40 to 43 volumes (i.e., from 2 min to 2 min 9 s).

Table 3
Clusters of significant group activation in response to olfactory stimuli.

Odor≥Air				NIH (mm) [a]				
Voxels	Peak region	*p* value	*z*-max	*x*	*y*	*z*	Olfactory Regions Covered	Areas Outside Olfactory Network
25922	Right Crus II	< 0.001	4.26	59	−78	−49	Right Hippocampus	Left Crus I; Right Crus I; Left Crus II; Left VIIb; Right VIIb; Right VIIIa
7148	Right Hippocampus	< 0.001	4.42	39	−14	−35	Amygdala laterobasal group; Amygdala superficial group; Hippocampus entorhinal cortex; Hippocampus subiculum; Frontal Orbital Cortex; Thalamus	Frontal Pole; Temporal Pole; Parahippocampal Gyrus anterior division; Pallidum
6626	Left Entorhinal cortex	0.001	3.89	6	−25	−38	Amygdala laterobasal group; Amygdala superficial group; Frontal Medial Cortex; Frontal Orbital Cortex; Hippocampus	Frontal Pole; Temporal Pole; Parahippocampal Gyrus anterior division; Pallidum
6264	Cingulate Gyrus posterior division	0.002	4.24	23	−55	9	Right Hippocampus	Precentral Gyrus; Juxtapositional Lobule Cortex (formerly Supplementary Motor Cortex); Cingulate Gyrus anterior division; Precuneous Cortex; Pallidum
5559	Right Hippocampus	0.005	3.66	64	−63	28		Superior Parietal Lobule; Angular Gyrus; Lateral Occipital Cortex superior division; Precuneous Cortex; Cuneal Cortex; Occipital Pole; Pallidum
4737	Right Pallidum	0.012	3.54	39	−1	26	Right Hippocampus	Frontal Pole; Superior Frontal Gyrus; Middle Frontal Gyrus; Juxtapositional Lobule Cortex (formerly Supplementary Motor Cortex); Paracingulate Gyrus; Cingulate Gyrus anterior division

NIH = National Institutes of Health.
[a] Coordinates listed are relative to the study-specific pediatric template included in supplementary materials (Fonov et al., 2011; Fonov et al., 2009). Results of the statistical contrast Odor > Air. Brain regions included within each significant cluster were separated into two different columns according to whether they were within or outside the olfactory network. *P* values are whole brain cluster threshold corrected for multiple comparisons using a minimum voxel height of *z* 2.3.

The entire imaging protocol including the scout, MPRAGE, verbal instructions, the odor exposure fMRI scan, calibration of respiration trace, shimming and scan reconstruction takes 10 min on average.

2.6. Data processing

MRI data preprocessing was performed using FSL (http://www.fmrib.ox.ac.uk/fsl/), AFNI (http://afni.nimh.nih.gov/afni/) and ANTS (https://www.nitrc.org/projects/ants/). Our preprocessing pipeline consisted of (1) motion correction, (2) spike artifact removal, (3) high-pass filtering [sigma = 50s], and (4) spatial smoothing [FWHM = 5mm]. The mean time series from the ventricles was extracted, and along with rigid body motion parameters and single-point motion regressors (framewise displacement and dvars calculated via fsl_motion_outliers), was included as a nuisance regressor. To reduce the effects of head motion, participants with a mean absolute motion value (RMS, as calculated by FSL mcflirt) greater than 1.0 were excluded (n = 5). The remaining subjects' mean absolute motion ranged from 0.082 to 0.764, with a group mean of 0.282 and standard deviation of 0.222.

Time series analyses were carried out using FILM with local autocorrelation correction (Woolrich et al., 2001). Condition effects were estimated at each voxel yielding the following contrasts for each participant: Odor > Air, Air > Odor. FMRI data were registered to the MPRAGE and then warped to the study-specific pediatric template (template included in supplementary materials; (Fonov et al., 2011, 2009) via ANTS diffeomorphic registration (Avants et al., 2011).

2.7. Creation of POC and SOC masks

Masks of the individual brain structures within the POC and SOC were created using published atlases or hand-drawn according to the neuroanatomical literature (see Fig. 3; masks available upon request). Atlas-based masks were warped from the 2mm MNI152 template to our pediatric template using ANTS diffeomorphic registration (Avants et al., 2011). The following masks were chosen for the POC: 1) left and right piriform cortex, hand-drawn on the MNI152 standard brain as illustrated by Mai et al. (2008), then warped to our pediatric template brain; 2) the left and right POC amygdala (including the periamygdaloid region, anterior and posterior nuclei, nucleus of the lateral olfactory tract, and the medial nucleus (Gottfried and Zald, 2005; Sah et al., 2003), all of which are included in the centromedial and superficial amygdala subdivisions in the Jülich histological (cyto- and myeloarchitectonic) atlas (Amunts et al., 2005), these subregions were thresholded at 50% probability, binarized and combined; 3) left and right entorhinal cortex masks, also obtained from the Jülich atlas and thresholded at 50% probability (Amunts et al., 2005). SOC masks included: 1) left and right lateral OFC (created by combining the middle, superior, and inferior orbital frontal regions from the Automated Anatomical Labeling atlas (AAL; Tzourio-Mazoyer et al., 2002); 2) medial OFC (created by combining the left and right medial OFC masks from the AAL atlas (Tzourio-Mazoyer et al., 2002) in order to capture the olfactory areas of the OFC, as described in Gottfried and Zald (2005); 3) left and right insular cortex (from the AAL atlas); 4) left and right hippocampus (from the AAL atlas); 5) SOC amygdala (including the lateral nucleus) represented using the Jülich laterobasal amygdala subregion mask, thresholded at 50%); and finally 6) left and right thalamus (created from the Harvard-Oxford subcortical atlas, thresholded at 50%) (Desikan et al., 2006; Frazier et al., 2005).

2.8. Data analysis – Group-level

Analyses of olfactory activation group-wise effects were conducted using a whole-brain, mixed-effects FLAME 1+2 (FMRIB's Local Analysis of Mixed Effects) analysis. *Z*-statistic images were whole-brain corrected for multiple comparisons using a cluster threshold correction

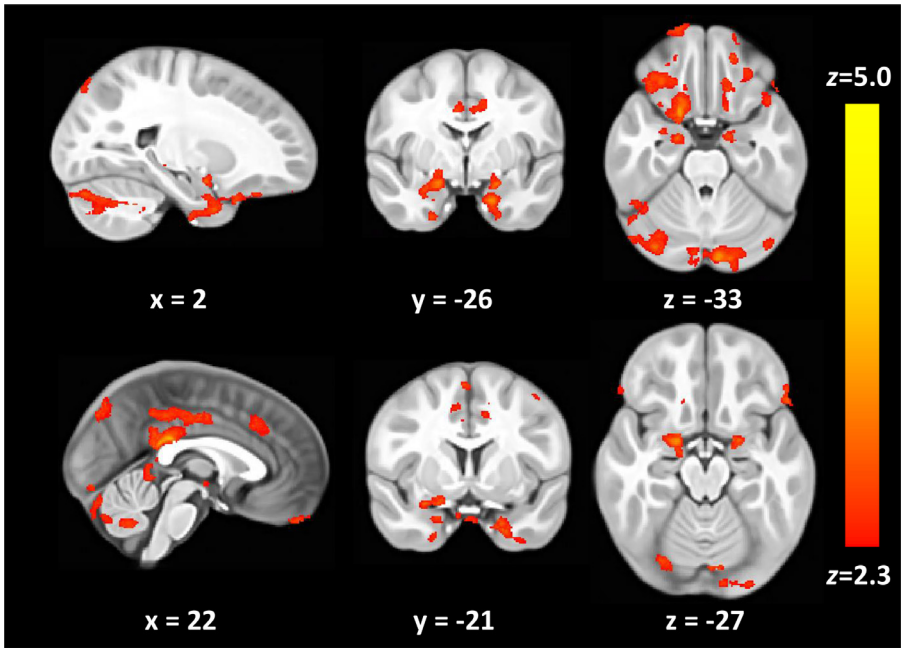

Fig. 4. Brain activation in response to odor stimulation. Clusters signify significant brain activation for the contrast Odor > Air, following whole-brain correction for multiple comparisons (voxel height = z 2.3, cluster threshold $p < 0.05$. Images are shown in radiological convention (R = L). The activation map in nifit format can be found in our Supplementary Materials.

Table 4
Brain-region specific activation characteristics within POC and SOC extracted from the significant activation identified in the whole-brain analysis.

			NIH (mm)[a]						NIH (mm)[a]		
Left Hemisphere	# of active voxels	z-Max	x	y	z	Right Hemisphere	# of active voxels	z-Max	x	y	z
Medial OFC	1592/24203	3.70	33	17	−37	Medial OFC	1592/24203	3.70	33	17	−37
Entorhinal cortex	776/2627	3.886	6	−25	−38	Entorhinal cortex	656/3150	3.42	40	−29	−34
Hippocampus	36/3487	2.93	5	−54	−17	Hippocampus	107/3643	3.23	41	−30	−33
Inferior OFC	519/7763	3.49	5	−8	−37	Inferior OFC	1064/7852	3.524	54	1	−36
Insular Cortex	0/7414					Insular Cortex	0/7009				
Piriform Cortex	91/675	3.48	4	−25	−29	Piriform Cortex	442/700	3.68	40	−17	−36
POC Amygdala (CM & SF)	424/1796	3.58	3	−26	−28	POC Amygdala (CM & SF)	644/1522	3.90	39	−25	−27
SOC Amygdala (LB)	153/1587	3.69	5	−26	−39	SOC Amygdala (LB)	319/1485	3.28	41	−29	−33
Thalamus	169/6812	3.41	17	−36	−16	Thalamus	2/6718	2.56	27	−33	−17

[a] Coordinates from the study-specific pediatric template included in Supplementary Materials (Fonov et al., 2011; 2009). Active voxels = voxels with a z-value ≥ 2.3. OFC = orbital frontal cortex, POC = primary olfactory cortex, SOC = secondary olfactory cortex, CM = centromedial, SF = superficial, LB = laterobasal, NIH = National Institutes of Health. The results reported in this table only include voxels that were significant in our whole brain analysis. Activation in specific regions is provided for descriptive purposes only.

with the individual voxel threshold at $z = 2.3$ and a corrected cluster significance threshold of $p < 0.05$ (Worsley, 2001). To test whether the fMRI protocol is sensitive to individual differences in olfactory processing, we also analyzed the relationship between olfactory activation (i.e., the Odor > Air contrast) and olfactory detection threshold as measured by the Sniffin' Sticks (Hummel et al., 1997) odor detection Threshold Test; to this end, a second analysis was run with Sniffin' Sticks Threshold Test scores entered as a covariate in the model. As above, z-statistic images were whole-brain corrected for multiple comparisons using a cluster threshold correction with the individual voxel threshold at $z = 2.3$ and a corrected cluster significance threshold of $p < 0.05$ (Worsley, 2001). In addition to the whole brain analysis, a region of interest correlational analysis, limited to POC regions that were hypothesized to be related to olfactory detection threshold were also conducted.

To more precisely describe significant, whole brain activation clusters within the POC and SOC, FSL's Featquery and fslstats were used to query the thresholded z-stat image for the group-level contrast Odor > Air. The following metrics were obtained for each mask within the POC and SOC (see above): the maximum z-value, the coordinates of the peak z-value, and the number of voxels activated above the $z = 2.3$ threshold within each mask. Note that there were other brain regions outside of the POC and SOC that showed significant activation at the group-level, but as they were not included in our a priori model, they are not further detailed using this analytical approach.

3. Results

3.1. fMRI group-level analyses

Group analyses conducted using a whole-brain field-of-view yielded significant activation across POC and SOC (Table 3/Fig. 4). Follow-up inquiry via FSL's Featquery indicated that our olfactory stimulation task elicited significant activation in 16/17 areas of interest (Table 4).

3.2. Relationship between olfactory activation and odor detection ability

The analysis of the relationship between olfactory activation and olfactory detection threshold showed that Sniffin' Sticks scores on the Threshold Test (where lower scores indicate a higher odor detection threshold) were positively correlated with the right superficial amygdala region and inversely correlated to right frontal cortex, posterior insula, occipital, and cerebellar activation (Fig. 5 and Table 5). That is, participants who are less able to detect odorants at low concentrations tended to show greater activation across cortical and cerebellar brain regions while stronger activation in the amygdala was associated with

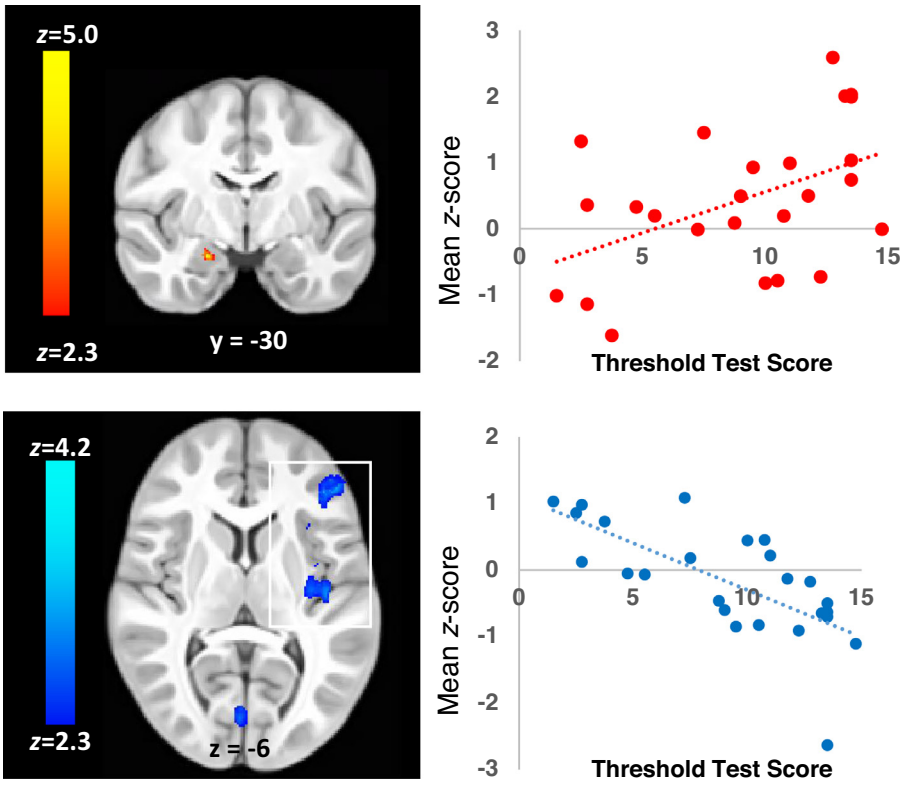

Fig. 5. The relationship between odor detection threshold and activation in the right superficial subregion of the amygdala (top) and frontal and insular regions (bottom). The scatter plots shows the mean activation for individual subjects within the significant cluster in the right amygdala and left frontal and insular cortex (boxed in white) plotted against the score of the Threshold Test from the Sniffin Sticks battery. Lower Sniffin' Sticks Threshold Test scores indicate a higher olfactory detection threshold and therefore poorer ability to detect odorants at low concentrations. Images are shown in radiological convention (R = L).

better smell detection ability.

4. Discussion

The present study used a short, passive, fMRI protocol with individualized stimulus timing to address the difficulties involved in imaging olfactory network functioning and in conducting fMRI research on children. We detected and characterized robust patterns of olfactory activation across areas of the primary and secondary olfactory cortex in a sample of school-aged children. Moreover, we delineated the varied patterns of activation across participants and regions of interest at the individual level. Finally, we demonstrated that our method was sufficiently sensitive and robust to characterize a relationship between olfactory activation and olfactory detection threshold in typically developing children. These three findings highlight the feasibility of olfactory fMRI studies focusing on earlier stages of development, and across different clinical populations.

4.1. Activation in primary and secondary olfactory areas

The present study detected activation in both primary and secondary olfactory areas. Namely, we detected olfactory activity in the piriform cortex, the amygdala, lateral OFC, medial OFC, entorhinal cortex, insula, thalamus, and hippocampus; an improvement in coverage and specificity compared to a previous pediatric study. To our knowledge, Hummel et al. (2012) is the only previous study that used fMRI to study olfactory activation in children. Those investigators detected a pattern of olfactory activation in piriform cortex, amygdala, and hippocampus among children ranging from 9 to 12 years of age. It is possible that the more limited activation reported by Hummel's group is related to differences in the odorant exposure methods. As opposed to our stimulus release timing that was optimized based on individual respiration patterns, the study by Hummel and colleagues released the odorant at fixed time intervals, introducing the possibility of the odorant being released during exhalation, which would likely result in lower power to detect brain activity. Additional information about the reliability of activation at the individual level can be found in the supplementary information section.

Differences in length of total odorant exposure also may have contributed to differences in results between the two studies. Hummel used three, 3-min runs each presenting an unpleasant smell (sweat or rotten eggs) during six 15-sec "ON" blocks with short stimulus release (1 s) and inter-trial intervals (2 s) and alternated this with six "OFF" blocks absent of stimulus. Our study, on the other hand, used one pleasant odor during four 9-sec trials with at least 18 sec ITI (depending on participant respiration rate) totaling a minimum task duration of 1 min and 48 s. The children in Hummel's study were exposed to the odorant for a total of 90 s while the children in our study were exposed to the odorant for a total of 36 s. It is possible that children habituate to odors more rapidly than adults and, hence, the implementation of a very short activation paradigm allowed us to observe more consistent activation across the POC and SOC. Additionally, a shorter total task time is more clinically feasible when scanning children, as they have shorter attention spans and higher protocol-related anxiety which may affect head motion. We believe that we were able to elicit and measure stronger activation in the POC and SOC because individualized release timing allows for more precise olfactory stimulation and because a longer inter-trial interval, coupled with shorter overall exposure, addresses the inherent challenges presented by rapid olfactory habituation.

4.2. Olfactory activation and olfactory detection threshold

We hypothesized that individuals who can detect odorants at the lowest concentrations would show the highest levels of activation in the POC during our fMRI odor paradigm. This hypothesis was partially confirmed, with a positive correlation observed between smell detection ability and activation in the right amygdala superficial subregion. However, we also found that the relationship between odor detection ability and fMRI activation was primarily observed in brain regions outside of the POC and opposite to the hypothesized direction. In this sample of typically developing children, those participants who showed greater levels of activation in the frontal, occipital, insular, and

Table 5
Regions showing a correlation between odor activation and Sniffin' Sticks Threshold Test scores.

Voxels	+/−	*p*	z-Max	MNI (mm)[a] *x*	*y*	*z*	Peak region	Other regions
216	+	0.034[b]	3.82	41	−30	−30	Amygdala superficial	Amygdala laterobasal, hippocampus
6545	−	0.002	4.2	−18	19	−15	Frontal Pole	Insula; Middle Frontal Gyrus; Inferior Frontal Gyrus pars triangularis; Inferior Frontal Gyrus pars opercularis; Frontal Operculum Cortex; Central Opercular Cortex
6536	−	0.002	3.94	−12	−98	−26	Occipital Fusiform Gyrus	Lateral Occipital Cortex inferior division; Intracalcarine Cortex; Lingual Gyrus; Temporal Occipital Fusiform Cortex; Pallidum; Hippocampus; Left VI; Vermis VI; Right VI; Left Crus I

[a] Coordinates from the study-specific pediatric template included in supplementary materials (Fonov et al., 2011, 2009).
[b] Region of interest analysis.

cerebellar regions also showed higher olfactory detection thresholds as assessed by the Sniffin' Sticks Threshold Test; that is, lower levels of activation were observed in those children who were better able to detect odorants at low concentrations, suggesting more rapid habituation in cortical and cerebellar regions may occur in these children. Notably, similar, inverse relationships between fMRI activation and level of expertise have been previously reported in perfumers (Plailly et al., 2012), which suggests that neural adaptations resulting in lower BOLD activation may be a generalizable neural signature across various olfactory domains.

4.3. Olfactory circuitry and development

Our odor paradigm has the potential to improve our understanding of the development of olfactory processing abilities in humans. Olfactory processing is unique compared to other sensory modalities, as olfactory receptor neurons project to the olfactory bulb, and then directly to the olfactory cortex, which includes the SF subregion of the amygdala (Wilson, 2009), piriform cortex, entorhinal cortex, and the OFC. It is the only sensory modality that does not have an intermediary projection between the thalamus and the cerebral cortex (Sarnat et al., 2017) and is the earliest sense to develop, with function beginning prenatally before neuroanatomical and metabolic maturation is fully reached. For example, preterm neonates respond to olfactory stimuli after 28 weeks gestation (Sarnat et al., 2017) and olfactory reflexes can be tested in infants born at term. Furthermore, olfaction has been shown to have important metabolic roles, which is critically important in the care of very preterm infants (Bloomfield et al., 2017). The approach described in this paper can be used to link the development of olfactory processing at the very earliest ages with neuroimaging findings. Combining functional imaging techniques with clinical olfactory responses is critical for forwarding our understanding of how the development of the olfactory network relates to development of olfaction and related processes.

4.4. Limitations

First, our study used a passive odorant exposure paradigm that did not include task or memory components while collecting fMRI data. This was done to develop a technique that could be used across a wide range of participants, including nonverbal individuals (e.g., infants), individuals with significant cognitive impairment, and individuals with severe developmental disabilities. Thus, we are unable to comment on possible effects on BOLD activation that may be produced by task alterations. Secondly, our study utilized a single odorant. This stimulus, a rose-like, phenyl ethyl alcohol odorant, was chosen because it specifically stimulates the olfactory system, but not the somatosensory trigeminal system. Therefore, it is unclear whether unpleasant odorants such as hydrogen sulfide, which is also strictly processed by the olfactory system, would elicit the same activation effects. It is unknown how much the valence of the stimulus affected the results, as odors like hydrogen sulfide are considered to have a negative valence and the currently-used rose-like smell is considered positive. Third, our sample had an unequal sex distribution with 19 male and 6 female participants. Because of the small number of females, it remains unclear how our sex distribution affected these results. Future studies comprising adequately powered subsamples of each sex will help to address this consideration. Lastly, it is important to consider that four of the children included in this sample performed in the hyposmic range on the Threshold Test and one child performed in the microsmic range on the UPSIT. While there were no other indications of olfactory impairment reported by the participants or their parents, these findings were unexpected and may have influenced our fMRI results.

5. Conclusion

The olfactory stimulation paradigm we describe was well-tolerated by typically developing children and demonstrated the feasibility of measuring robust olfactory brain activation by fMRI in this population. Using brain imaging techniques to study olfactory function in typically developing children holds promise for studying more challenging populations of infants and children having developmental concerns where odor perception may be specifically affected. Focusing on brain biomarkers, such as we describe in this report, may help to characterize olfactory developmental pathways both for typical and atypical olfactory processing, and aid in early identification of conditions that develop during childhood, such as ASD, as well as conditions that develop later in life, such as Parkinson's disease and Alzheimer's disease. Moreover, our study was able to show that olfactory detection threshold is associated with olfactory activation in typically developing children, opening up the possibility of studying other factors such as cognition, socioemotional behavior, and developmental characteristics in early developmental stages and across populations that would present higher levels of variability. Furthermore, coupling improved experimental stimulus delivery with advances in imaging technology, such as ultra-fast imaging fMRI (Posse et al., 2013), our methodology shows potential for expanding what is known about temporal response patterns across olfactory networks, possibly assisting in the characterization of each olfactory region's role within the networks.

Funding

This work was supported by the National Institutes of Health [NIMH R01-MH104313].

Conflict of interest

None.

Supplementary materials

Supplementary material associated with this article can be found, in the online version, at doi:10.1016/j.pscychresns.2018.11.011.

References

Amunts, K., Kedo, O., Kindler, M., Pieperhoff, P., Mohlberg, H., Shah, N.J., et al., 2005. Cytoarchitectonic mapping of the human amygdala, hippocampal region and entorhinal cortex: intersubject variability and probability maps. Anat. Embryol. 210, 343–352.

Atanasova, B., Graux, J., El Hage, W., Hommet, C., Camus, V., Belzung, C., 2008. Olfaction: a potential cognitive marker of psychiatric disorders. Neurosci. Biobehav. Rev. 32, 1315–1325.

Avants, B.B., Tustison, N.J., Song, G., Cook, P.A., Klein, A., Gee, J.C., 2011. A reproducible evaluation of ANTs similarity metric performance in brain image registration. NeuroImage 54, 2033–2044.

Bloomfield, F.H., Alexander, T., Muelbert, M., Beker, F., 2017. Smell and taste in the preterm infant. Early Hum. Dev. 114, 31–34.

Croy, I., Symmank, A., Schellong, J., Hummel, C., Gerber, J., Joraschky, P., et al., 2014. Olfaction as a marker for depression in humans. J. Affect. Disord. 160, 80–86.

Daivs, A.S., 2006. The neuropsychological basis of childhood pathology. Psychol. Sch. 43, 503–512.

Dapretto, M., Davies, M.S., Pfeifer, J.H., Scott, A.A., Sigman, M., Bookheimer, S.Y., et al., 2006. Understanding emotions in others: mirror neuron dysfunction in children with autism spectrum disorders. Nat. Neurosci. 9, 28–30.

Davidson, M.C., Thomas, K.M., Casey, B.J., 2003. Imaging the developing brain with fMRI. Ment. Retard. Dev. Disabil. Res. Rev. 9, 161–167.

de Olmos, J., Hardy, H., Heimer, L., 1978. The afferent connections of the main and the accessory olfactory bulb formations in the rat: an experimental HRP-study. J. Comp. Neurol. 181, 213–244.

Desikan, R.S., Segonne, F., Fischl, B., Quinn, B.T., Dickerson, B.C., Blacker, D., et al., 2006. An automated labeling system for subdividing the human cerebral cortex on MRI scans into gyral based regions of interest. NeuroImage 31, 968–980.

Doty, R.L., 2007. Olfaction in Parkinson's disease. Parkinsonism Relat. Disord. 13 (Suppl 3), S225–S228.

Doty, R.L., Brugger, W.E., Jurs, P.C., Orndorff, M.A., Snyder, P.J., Lowry, L.D., 1978. Intranasal trigeminal stimulation from odorous volatiles: psychometric responses from anosmic and normal humans. Physiol. Behav. 20, 175–185.

Doty, R.L., Shaman, P., Kimmelman, C.P., Dann, M.S., 1984. University of Pennsylvania smell identification test: a rapid quantitative olfactory function test for the clinic. Laryngoscope 94, 176–178.

Emerson, R.W., Adams, C., Nishino, T., Hazlett, H.C., Wolff, J.J., Zwaigenbaum, L., et al., 2017. Functional neuroimaging of high-risk 6-month-old infants predicts a diagnosis of autism at 24 months of age. Sci. Transl. Med. 9.

Fonov, V., Evans, A.C., Botteron, K., Almli, C.R., McKinstry, R.C., Collins, D.L., 2011. Unbiased average age-appropriate atlases for pediatric studies. NeuroImage 54, 313–327.

Fonov, V., Evans, A.C., Botteron, K., Almli, C.R., McKinstry, R.C., Collins, D.L., et al., 2009. Unbiased nonlinear average age-appropriate brain templates from birth to adulthood. NeuroImage 47.

Forbes, E.E., Christopher May, J., Siegle, G.J., Ladouceur, C.D., Ryan, N.D., Carter, C.S., et al., 2006. Reward-related decision-making in pediatric major depressive disorder: an fMRI study. J. Child Psychol. Psychiatry Allied Discip. 47, 1031–1040.

Frasnelli, J., Hummel, T., Berg, J., Huang, G., Doty, R.L., 2011. Intranasal localizability of odorants: influence of stimulus volume. Chem. Senses 36, 405–410.

Frazier, J.A., Chiu, S., Breeze, J.L., Makris, N., Lange, N., Kennedy, D.N., et al., 2005. Structural brain magnetic resonance imaging of limbic and thalamic volumes in pediatric bipolar disorder. Am. J. Psychiatry 162, 1256–1265.

Gottfried, J.A., Zald, D.H., 2005. On the scent of human olfactory orbitofrontal cortex: meta-analysis and comparison to non-human primates. Brain Res. Brain Res. Rev. 50, 287–304.

Gottschlich, M., Hummel, T., 2015. Effects of handedness on olfactory event-related potentials in a simple olfactory task. Rhinology 53, 149–153.

Hilton, C.L., Harper, J.D., Kueker, R.H., Lang, A.R., Abbacchi, A.M., Todorov, A., et al., 2010. Sensory responsiveness as a predictor of social severity in children with high functioning autism spectrum disorders. J. Autism Dev. Disord. 40, 937–945.

Hummel, T., Hummel, C., Iannilli, E., Baur, A., Gerber, J., Chopra, A., 2012. Olfactory processing in children and young adults. Chemosens. Percept. 5, 128–137.

Hummel, T., Kobal, G., Gudziol, H., Mackay-Sim, A., 2007. Normative data for the "Sniffin' Sticks" including tests of odor identification, odor discrimination, and olfactory thresholds: an upgrade based on a group of more than 3,000 subjects. Eur. Arch. Oto-Rhino-Laryngol. 264, 237–243.

Hummel, T., Sekinger, B., Wolf, S.R., Pauli, E., Kobal, G., 1997. 'Sniffin' sticks': olfactory performance assessed by the combined testing of odor identification, odor discrimination and olfactory threshold. Chem. Senses 22, 39–52.

Iannilli, E., Stephan, L., Hummel, T., Reichmann, H., Haehner, A., 2017. Olfactory impairment in Parkinson's disease is a consequence of central nervous system decline. J. Neurol. 264, 1236–1246.

Iannilli, E., Wiens, S., Arshamian, A., Seo, H.S., 2013. A spatiotemporal comparison between olfactory and trigeminal event-related potentials. NeuroImage 77, 254–261.

Levitin, D.J., Menon, V., Schmitt, J.E., Eliez, S., White, C.D., Glover, G.H., et al., 2003. Neural correlates of auditory perception in Williams syndrome: an fMRI study. NeuroImage 18, 74–82.

Lorig, T.S., Elmes, D.G., Zald, D.H., Pardo, J.V., 1999. A computer-controlled olfactometer for fMRI and electrophysiological studies of olfaction. Behav. Res. Methods Instrum. Comput. 31, 370–375.

Luking, K.R., Repovs, G., Belden, A.C., Gaffrey, M.S., Botteron, K.N., Luby, J.L., et al., 2011. Functional connectivity of the amygdala in early-childhood-onset depression. J. Am. Acad. Child Adolesc. Psychiatry 50, 1027–1041.e1023.

Mai, J.K., Paxinos, G., Voss, T., 2008. Atlas of the Human Brain, 3rd ed. Academic Press, San Diego.

Martinez-Marcos, A., 2009. On the organization of olfactory and vomeronasal cortices. Prog. Neurobiol. 87, 21–30.

Moberg, P.J., Agrin, R., Gur, R.E., Gur, R.C., Turetsky, B.I., Doty, R.L., 1999. Olfactory dysfunction in schizophrenia: a qualitative and quantitative review. Neuropsychopharmacology 21, 325–340.

Mori, K., Sakano, H., 2011. How is the olfactory map formed and interpreted in the mammalian brain? Annu. Rev. Neurosci. 34, 467–499.

Murphy, C., Gilmore, M.M., Seery, C.S., Salmon, D.P., Lasker, B.R., 1990. Olfactory thresholds are associated with degree of dementia in Alzheimer's disease. Neurobiol. Aging 11, 465–469.

Pause, B.M., Miranda, A., Goder, R., Aldenhoff, J.B., Ferstl, R., 2001. Reduced olfactory performance in patients with major depression. J. Psychiatr. Res. 35, 271–277.

Philipsen, A., 2006. Differential diagnosis and comorbidity of attention-deficit/hyperactivity disorder (ADHD) and borderline personality disorder (BPD) in adults. Eur. Arch. Psychiatry Clin. Neurosci. 256 (Suppl 1), i42–i46.

Plailly, J., Delon-Martin, C., Royet, J.P., 2012. Experience induces functional reorganization in brain regions involved in odor imagery in perfumers. Hum. Brain Mapp. 33, 224–234.

Poellinger, A., Thomas, R., Lio, P., Lee, A., Makris, N., Rosen, B.R., et al., 2001. Activation and habituation in olfaction–an fMRI study. NeuroImage 13, 547–560.

Posse, S., Ackley, E., Mutihac, R., Zhang, T., Hummatov, R., Akhtari, M., et al., 2013. High-speed real-time resting-state FMRI using multi-slab echo-volumar imaging. Front. Hum. Neurosci. 7, 479.

Power, J.D., Mitra, A., Laumann, T.O., Snyder, A.Z., Schlaggar, B.L., Petersen, S.E., 2014. Methods to detect, characterize, and remove motion artifact in resting state fMRI. NeuroImage 84, 320–341.

Pruett Jr., J.R., Kandala, S., Hoertel, S., Snyder, A.Z., Elison, J.T., Nishino, T., et al., 2015. Accurate age classification of 6 and 12 month-old infants based on resting-state functional connectivity magnetic resonance imaging data. Dev. Cogn. Neurosci. 12, 123–133.

Sah, P., Faber, E.S., Lopez De Armentia, M., Power, J., 2003. The amygdaloid complex: anatomy and physiology. Physiol. Rev. 83, 803–834.

Sarnat, H.B., Flores-Sarnat, L., Wei, X.C., 2017. Olfactory development, part 1: function, from fetal perception to adult wine-tasting. J. Child Neurol. 32, 566–578.
Sobel, N., Prabhakaran, V., Zhao, Z., Desmond, J.E., Glover, G.H., Sullivan, E.V., et al., 2000. Time course of odorant-induced activation in the human primary olfactory cortex. J. Neurophysiol. 83, 537–551.
Tzourio-Mazoyer, N., Landeau, B., Papathanassiou, D., Crivello, F., Etard, O., Delcroix, N., et al., 2002. Automated anatomical labeling of activations in SPM using a macroscopic anatomical parcellation of the MNI MRI single-subject brain. NeuroImage 15, 273–289.
Wang, J., Sun, X., Yang, Q.X., 2014. Methods for olfactory fMRI studies: implication of respiration. Hum. Brain Mapp. 35, 3616–3624.
Wechsler, D., 1999. Wechsler Abbreviated Scale of Intelligence. The Psychological Corporation, New York.
Wilson, D.A., 2009. Olfaction as a model system for the neurobiology of mammalian short-term habituation. Neurobiol. Learn. Mem. 92, 199–205.
Woodberry, K.A., Seidman, L.J., Giuliano, A.J., Verdi, M.B., Cook, W.L., McFarlane, W.R., 2010. Neuropsychological profiles in individuals at clinical high risk for psychosis: relationship to psychosis and intelligence. Schizophr. Res. 123, 188–198.
Woolrich, M.W., Ripley, B.D., Brady, M., Smith, S.M., 2001. Temporal autocorrelation in univariate linear modeling of FMRI data. NeuroImage 14, 1370–1386.
Worsley, K.J., 2001. Statistical analysis of activation images. In: Jezzard, P., Matthews, P.M., Smith, S.M. (Eds.), Functional Magnetic Resonance Imaging: An Introduction to Methods. Oxford University Press, Oxford, pp. 251–270.
Yousem, D.M., Williams, S.C., Howard, R.O., Andrew, C., Simmons, A., Allin, M., et al., 1997. Functional MR imaging during odor stimulation: preliminary data. Radiology 204, 833–838.